



Comparative Analysis of Stiffness in Redundant Co-axial Spherical Parallel Manipulator Using Matrix Structural Analysis and VJM Method

Zakarya Chebili^{1,2} · Said Alem^{1,2} · Selman Djefal^{1,3}

Received: 13 July 2022 / Accepted: 22 February 2023 / Published online: 1 April 2023
© The Author(s), under exclusive licence to Shiraz University 2023

Abstract

Several studies have addressed stiffness analysis through different available methods including finite element analysis (FEA) and the virtual joint method (VJM) among others. However, matrix structural analysis (MSA) has not been used, although previous research has shown that it provides reliable results. Therefore, this paper focuses on the kineto-static analysis of a three-degree-of-freedom symmetrical parallel kinematic manipulator (PKM) with curved links, known as a spherical parallel manipulator (SPM). First, kinematic modeling is introduced through the inverse kinematic problem and the Jacobian matrix; then a detailed study of the stiffness modeling is established. Secondly, the force–deflection relationship is studied in the form of a numerical calculation and a graphical representation. Moreover, the kinematic redundancy is derived. Through MATLAB simulations, the deflection of the joints in both parts, translation, and rotation, is graphically represented using a numerical calculation method. Comparatively, SPM is purposefully compared to VJM in order to determine the efficiency of the proposed method. Interestingly, kinematic redundancy leads to better SPM performance, in which adding extra links (legs) to the robot strengthens the SPM structure and yields less joint deflection. It is worth noting that the MSA technique successfully deals with complex structures such as closed-loop chains, which is clearly apparent in the simplicity of its mathematical model toward the considered robot.

Keywords Spherical parallel manipulator · Stiffness analysis · Matrix structural analysis · Kinematic redundancy · Joint deflection

1 Introduction

Stiffness analysis of a mechanical structure is a significant area of focus in research nowadays. It refers to the impact of applied wrenches and external physical loads on the body of a mechanism, and how the structure reacts with respect to its accuracy and positioning errors (Pashkevich et al. 2011). In particular, industrial robots with serial, parallel, and hybrid kinematic architecture have become popular topics in many fields, such as manufacturing and machining tools, medical devices such as wrist and ankle rehabilitation devices (Martinez et al. 2013; Pehlivan et al. 2012), exoskeleton systems (Christensen and Bai 2018), haptic devices for teleoperation surgery (Saafi et al. 2013), and other applications. Parallel manipulators are intended to be used with more precision to enable a larger workspace, and to be strengthened compared to serial manipulators due to various advantages. On the other hand, closed-loop chains could be challenging in terms of kinematic modeling, stiffness analysis, and so on. Hence, this paper focuses on stiffness analysis of a

S. Alem and S. Djefal contributed equally to this work.

✉ Zakarya Chebili
z.chebili@univ-boumerdes.dz

Said Alem
alem-said@univ-boumerdes.dz

Selman Djefal
djaffal.selman@univ-oeb.dz

- ¹ Laboratory of Energetics, Mechanics and Engineering (LEMI), Department of Mechanical Engineering, University of M'hamed Bougera, Boumerdes, Boumerdes, Algeria
- ² Laboratory of Solid Mechanics and Systems, Department of Mechanical Engineering, University of M'hamed Bougera, Boumerdes, Boumerdes, Algeria
- ³ CMASMTF Laboratory, Department of Mechanical engineering, University of Oum El Bouaghi, Ain Beida, Algeria

three-degree-of-freedom parallel manipulator with spherical links (legs). To solve this problem, many studies have been conducted on a variety of methods to determine the stiffness modeling. We distinguish the most well-known methods in the literature, such as finite element analysis (FEA) (Taghvaeipour et al. 2010; Piras et al. 2005; Klimchik et al. 2012; Azulay et al. 2014), virtual joint method (VJM) (Pashkevich et al. 2009; Klimchik et al. 2017), matrix structural analysis (MSA) (Deblaise et al. 2006; Nagai and Liu 2008), and weighted topological graph-based MSA (Li et al. 2017). The FEA method is based on the subdivision of a physical model of the robot structure into smaller particles (parts), which are formed by a meshing technique. The MSA approach is based on FEA but is more accurate and practical in the case of kinematics manipulators with a closed-loop chain due to the redundancy of the degrees of freedom and a complex and time-consuming numerical calculation. The VJM is the most simplistic and limited approach and is built on the extension of the main rigid body with virtual joints according to the elastic deformation of its links, joints, and actuators. Previous research (Taghvaeipour et al. 2012; Popov et al. 2019; Cammarata 2016) has implemented the aforementioned approaches to solve the structural stiffness problem. Stiffness modeling of different types of kinematic parallel manipulators (PKMs) has been studied extensively; however, little research has been conducted to investigate the spherical parallel manipulator (SPM). The general structure of an SPM is represented through the MSA technique for medical application, namely a rehabilitation instrument (Popov et al. 2019). SPM robots play an important role in medical applications, including rehabilitation devices and teleoperation instruments for surgery, due to the high precision that the mechanisms can offer, as well as their ability to perform complex motion and orientation in three-dimensional space. Recent contributions to the MSA technique include the work of Wu et al. (2014), who surveyed stiffness analysis modeling of different types of SPMs using the VJM approach. Further, Castigliano's theorem is reported for calculating the limb deflection. Thus, this paper aims to delve into stiffness analysis modeling of a three-degree-of-freedom coaxial SPM which is dedicated to medical field application when applying the MSA technique, where one of the complicated constraints is to kinematically model the SPM's structure due to its complex quadratic equation system. Hence, the MSA method is based on the obtained kinematics modeling. In addition, the force–deflection relationship is represented with regard to translation and orientation deflection, and a comparison study is carried out to validate the proposed approach. The rest of the paper is organized as follows: Section 2 presents a detailed kinematic analysis. Section 3 covers the stiffness modeling for the proposed computer-aided design (CAD) of the coaxial SPM. Section 4 presents the obtained results and discussion. Section 5

summarizes the main contributions. Finally, Sect. 6 is dedicated to a comparison study with VJM method.

2 Kinematic Analysis Modeling

Kinematic analysis is an important step in modeling robotics manipulators before CAD design. Parallel kinematic manipulators are more challenging to model than serial manipulators due to their closed-loop chains. A fundamental characteristic of a three-degree-of-freedom (DOF) SPM with revolute joints (R), as illustrated in Fig. 1, is the use of three identical kinematic chains with a curved linkage, and the links attach the mobile platform to the fixed platform. The center of rotation is located inside its kinematic structure as the gravity center which divides the robot structure into two symmetrical pyramids. Both platforms have the similar angles, v_i , while the three links that link the base platform have identical angles, α . Furthermore, γ and β are the angles of the orientation of the lower and upper regular pyramids, respectively. The joints of the fixed platform are known as proximal joints, and their axes are labeled by the unit vector u_i . The joints of the end effector are called the distal joints, its axis is a vector v_i , and the last set of joints between the proximal and distal links are called the intermediate joints; w_i is a unit vector applied to refer to its axes. Regarding the structure of the manipulator, it is connected in such a way that the axes of all the rotating joints intersect at a common point, which represents the center of the manipulator. The other choice of the coordinate system when analyzing the structure of the SPM is the most important issue. For example, Gosselin et al. (1994) obtained a simple solution

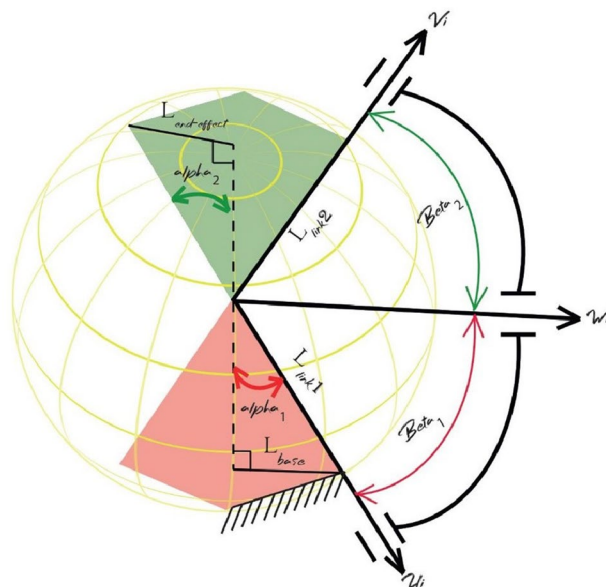


Fig. 1 Kinematics description of the i th leg of the SPM

of the direct kinematics of the SPM by taking advantage of the isotropy of the mechanism configuration where the axes of the joints of the fixed platform coincide with the Cartesian coordinates. In this case, the end effector moves with the mobile platform, namely the coordinate system and the convention.

2.1 Coordinate System

The coordinate system is considered to adequately represent all motions in practice. Therefore, the 12 sets of Euler angles cannot be applied. A new and less familiar coordinate representation, called tilt and twist angle, is used to describe the orientation of the motions of the complicated mechanism. In Bonev and Ryu (2001), the accessible workspace of a six-DOF parallel manipulator is represented in terms of the modified Euler angles, and in Bonev et al. (2002), this method is applied for symmetric mechanisms. The rotation matrix of tilt and torsion can be expressed in Eq. (1):

$$R(\phi, \theta, \sigma) = \begin{bmatrix} c\phi c\theta c(\sigma - \phi) - s\phi s(\sigma - \phi) & -c\phi c\theta s(\sigma - \phi) s\phi c(\sigma - \phi) & c\phi c\theta \\ s\phi c\theta c(\sigma - \phi) - c\phi s(\sigma - \phi) & -s\phi c\theta c(\sigma - \phi) - c\phi s(\sigma - \phi) & s\phi s\theta \\ -s\phi c(\sigma - \phi) & s\phi s(\sigma - \phi) & c\theta \end{bmatrix} \tag{1}$$

Based on the Denavit–Hartenberg convention (Niyetkaliyev and Shintemirov 2014), the mobile platform takes the form of a successive multiplication from the robot's fixed base to the end-effector platform represented in Eq. (2):

$$T_{system} = \prod_{i=1}^3 T_{BP} \cdot T_{L1} \cdot T_{L2} \cdot T_{MP} \tag{2}$$

where T_{BP} and T_{MP} stand for the transformation matrix of the base and moving platform, respectively, while T_{L1} and T_{L2} represent the transformation matrix of curved links (link 1 and link 2). The resulting matrix product T_{system} is related to a vector u_i that represents the orientation axis for the actuated joints, as given by Eq. (3):

$$u_i = \begin{bmatrix} -\sin \eta_i \cdot \sin \gamma \\ -\sin \eta_i \cdot \sin \gamma \\ \cos \gamma \end{bmatrix} \tag{3}$$

η_i is formed at the base platform according to the symmetry of the upper and lower pyramids, thus it is denoted as in Eq. (4):

$$\eta_i = \frac{2(i - 1)\pi}{3} \tag{4}$$

Furthermore, the unit vector w_i can be calculated in terms of u_i , as described in Eq. (5):

$$w_i = \begin{bmatrix} -s\eta_i \cdot s\gamma \cdot c\alpha_1 + (c\eta_i \cdot s\theta_i - s\eta_i \cdot c\gamma \cdot c\theta_i) \cdot s\alpha_1 \\ -c\eta_i \cdot s\gamma \cdot c\alpha_1 + (c\eta_i \cdot s\theta_i - s\eta_i \cdot c\gamma \cdot c\theta_i) \cdot s\alpha_1 \\ -c\gamma \cdot c\alpha_1 + s\gamma \cdot c\theta_i \cdot s\alpha_1 \end{bmatrix} \tag{5}$$

where θ_i , ($i = 1, 2, 3$) is the angle of the three actuated motors.

The unit vector of the axis of the distal link v_i is a function of the orientation of the moving platform; thus,

$$v_i = T_{system} \cdot v_i^* \tag{6}$$

noting that the T_{system} is the aforementioned rotation matrix, and v_i^* is the unit vector of the axis of the top link joints.

2.2 Inverse Kinematic Problem

The orientation and position of the moving platform (robot's end-effector) are expressed using the inverse kinematic

problem (IKP). In general, inverse kinematics is much easier to solve in the case of parallel kinematic manipulators. Most often, inverse kinematics in the case of PKMs is carried out on its geometry configuration and its structural features; likewise, the most known geometric approach is the vector method, which is a well-known method. Moreover, for a parallel robot with a spherically geometric structure, there are some geometric properties (all dimensions that characterize the architecture structure, namely, the mechanism's height, proximal and distal link dimensions and curved angles, and the radius of the fixed and mobile platforms) that are different from the ordinary general SPM architecture. Under the selected coordinate system, the unit vector u_i as prescribed in Eq. (3), for the case of a closed-loop chain of the SPM, is given in Eq. (7):

$$w_i \cdot v_i = \cos \alpha_2 \tag{7}$$

with ($i = 1, 2, 3$). Equation (8) defines the relationship between the proximal and distal links:

$$A \cdot x_i^2 + 2B \cdot x_i + C = 0 \tag{8}$$

In order to solve the polynomial equations system that is developed using the angle tangent identities and which can be expressed by Eq. (9):

$$\begin{cases} \cos \theta_i = \frac{1-t_i^2}{1+t_i^2} \\ \sin \theta_i = \frac{2t_i}{1+t_i^2} \\ t_i = \frac{\theta_i}{2} \end{cases} \quad (9)$$

We get the quadratic form as reported in Eq. (10):

$$A.t_{\theta_i}^2 + 2B.t_{\theta_i} + C = 0 \quad (10)$$

with the coefficients presented in Eq. (11)

$$\begin{cases} A = -v_{iy} \cdot \sin \alpha_1 - v_{iz} \cdot \cos \alpha_1 - \cos \\ B = v_{ix} \cdot \sin \alpha_1 \\ C = v_{iy} \cdot \sin \alpha_1 - v_{iz} \cdot \cos \alpha_1 - \cos \alpha_2 \end{cases} \quad (11)$$

where v_{ix} , v_{iy} , and v_{iz} are the components of the vector v_i . In a more explicit form, we can write v_i as in Eq. (12):

$$v_i = [v_{1x}, v_{1y}, v_{1z}, v_{2x}, v_{2y}, v_{2z}, v_{3x}, v_{3y}, v_{3z}] \quad (12)$$

The inverse kinematics problem is presented as an easy-to-follow algorithm. It was first developed by Tursynbek and Shintemirov (2021). Equation (10) represents a system of quadratic equations, which require an analytical development (Gosselin and Lavoie 1993).

2.3 Workspace Analysis

Workspace analysis is one of the most important parts of studying the robot's kinematics and allows one to represent all possible sets of points (volume) that the robot's end effector can reach. More importantly, workspace modeling of a parallel kinematic manipulator such as our case of study (coaxial SPM and general structure SPM) can be used as an

effective tool to optimize the considered robots by determining their singularity volume.

Basically, two main types of SPM structure are represented through the (ZYZ) axis, and since the workspace is essentially based on its developed inverse kinematics, real solutions express the reachable workspace, while unreal solutions demonstrate a singularity set of points. The graphical representation shows the workspace of both SPM structures, where Figs. 2 and 3 represent the general SPM architecture and the proposed coaxial SPM workspace, respectively. Both figures are divided into two main sections, where the green color refers to the reachable workspace area, whereas the red color section refers to the singularity volume area.

It can be noted that the singularity volume of the coaxial SPM is reduced compared to the general SPM structure. The Cartesian workspace shows a full three-dimensional (3D) set of points representing all possible points that the mobile platform can reach. The solutions of Eq. (10) are graphically represented in Figs. 2 and 3, which is a half sphere-like shape.

2.4 Jacobian Matrix

We have established so far the mathematical modeling of both inverse and forward kinematics of the 3-RRR SPM. The focus of this section is to determine the mechanism's Jacobian matrix. Basically, the Jacobian matrix can be derived from the relationship between the static forces of the robot's manipulator and its velocities. The Jacobian matrix of the 3-RRR spherical coaxial parallel manipulator is represented in Eq. (13):

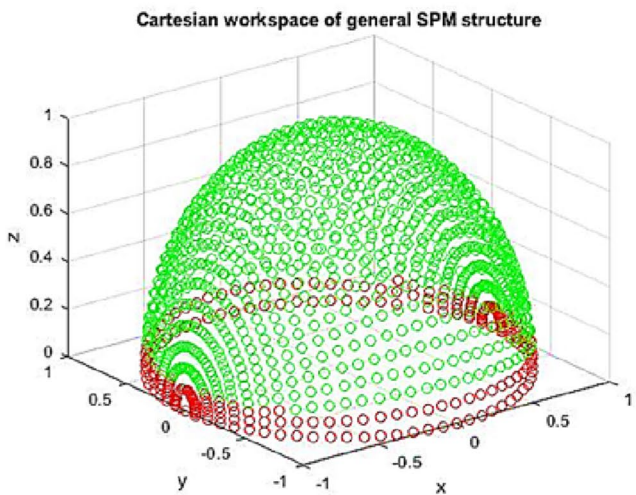
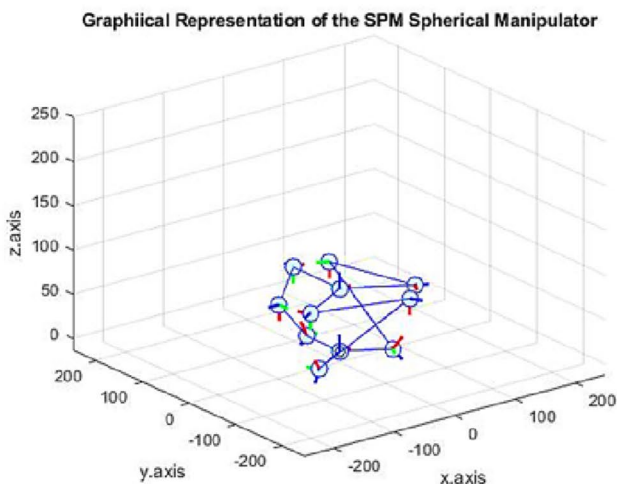


Fig. 2 Cartesian workspace of general SPM

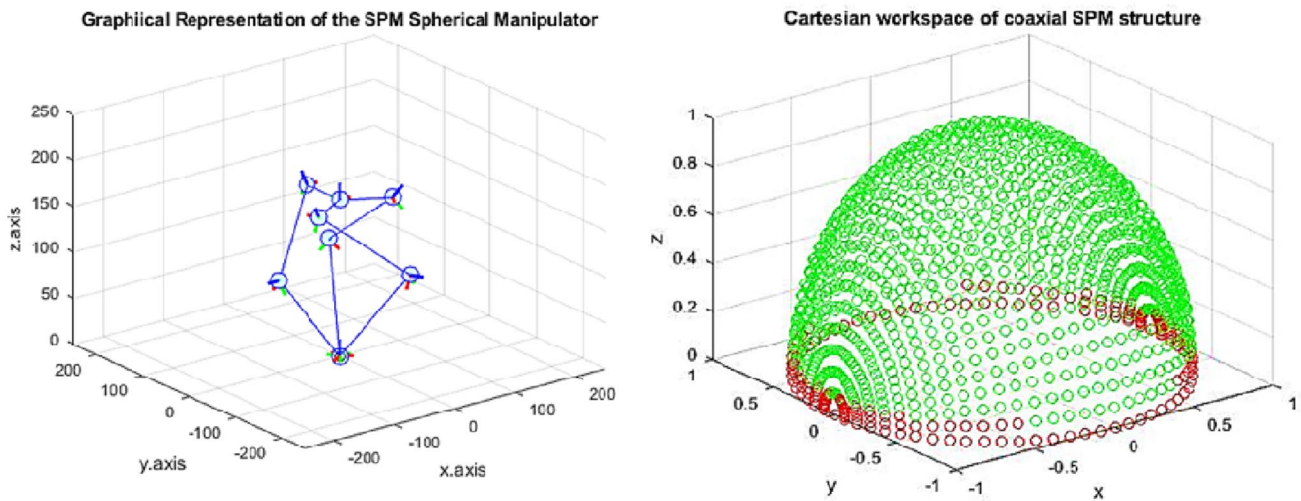


Fig. 3 Cartesian workspace of coaxial SPM

$$\dot{\theta} = J.\omega \tag{13}$$

To emphasize, Eq. (13) refers to the angular velocity vector of the mobile platform, and is the Jacobian matrix that connects the actuated joints vector. In general, the Jacobian matrix of parallel kinematic manipulators can be derived from the differentiation of its inverse kinematics. Thus, differentiating both sides of Eq. (7), we get the following Eq. (14):

$$\dot{\omega}_i v_i + \omega_i \dot{v}_i = 0 \tag{14}$$

with

$$\begin{cases} \dot{v}_i = \omega v_i \\ \dot{\omega}_i = \dot{\theta}.u_i \end{cases} \tag{15}$$

As expressed in Gosselin and Lavoie (1993), the Jacobian matrix can be also defined as in Eq. (16):

$$J = -J_2^{-1}.J_1 \tag{16}$$

In a more simplified mathematical representation, we can describe the Jacobian matrix with Eq. (17):

$$J_1 \omega + J_2 \dot{\theta} = 0 \tag{17}$$

with

$$J_1 = \begin{bmatrix} (w_1 \times v_1)^T \\ (w_2 \times v_2)^T \\ (w_3 \times v_3)^T \end{bmatrix} \tag{18}$$

$$J_2 = \text{diag}(w_1 \times u_1.v_1, w_2 \times u_2.v_2, w_3 \times u_3.v_3) \tag{19}$$

3 Stiffness Analysis

Mechanical structures such as robotic applications and industrial mechanisms depend on external wrenches (force and moment). These applied forces can affect their kinematic and dynamic behavior, causing singular states within the robot’s workspace, making it difficult to control the robot. Thus, stiffness modeling plays an important role in the design of any mechanical structure. It allows engineers to achieve an optimal design for a predefined task. However, to conduct mechanical stiffness analysis, it is recommended to use an appropriate method that relies on a simple calculation, which provides an accurate and resilient method that can handle multiple cases (flexible or rigid body, active or passive joints, open or closed-loop chains) (Klimchik et al. 2019). For this reason, the MSA technique is derived to calculate the stiffness of a spherical parallel manipulator (SPM) with three degrees of freedom. In addition, the force–displacement relationship is established to demonstrate the physical meaning of the application of external forces to the studied mechanism. Thus, the translational and rotational displacements of the joints are represented in numerical and graphical results.

3.1 Compliance Matrix Formulation of a Curved Beam

Usually, to determine the stiffness matrix of a mechanical structure, we simply use the FEA method with numerical software (e.g., MATLAB®), Ansys®), Solidworks®), etc.) which returns a ready-to-use system of equations of the studied mechanism. Its advantage is the known geometry of the robot’s links. On the other hand, parallel kinematic manipulators with

curved linkages require different approximations. Therefore, to derive the stiffness model of each curved link, Euler–Bernoulli beam theory is derived. In this regard, Fig. 4 shows a curved beam element acted upon by external wrenches.

In order to calculate the stiffness of the SPM limb, the compliance of a circular curved beam needs to be formulated. Figure 2 shows a cantilever with forces and moments applied onto the free end, and the compliance matrix is calculated using Euler–Bernoulli beam theory. The strain energy is expressed to complete this calculation.

$$U = \frac{R}{2} \int_0^\alpha \left[\frac{(f'_1)^2}{EA} + \frac{(f'_2)^2}{GA} + \frac{(f'_3)^2}{GA} + \frac{(m'_4)^2}{GI_x} + \frac{(m'_5)^2}{EI_y} + \frac{(m'_6)^2}{EI_z} \right] d\Phi \tag{20}$$

The applied forces and moments can be presented as

$$\begin{aligned} f'_1 &= f_1 \cos \phi - f_2 \sin \phi \\ f'_2 &= f_1 \sin \phi + f_2 \cos \phi \\ f'_3 &= f_3 \\ m'_4 &= m_4 \cos \phi - m_5 \sin \phi - f_3 R(1 - \cos \phi) \\ m'_5 &= m_4 \sin \phi - m_5 \cos \phi - f_3 R \sin \phi \\ m'_6 &= m_6 - f_1 R(1 - \cos \phi) - f_2 R \sin \phi \end{aligned} \tag{21}$$

Differentiating Eq. (20), we obtain the translational and rotational deflections based on Castigliano’s theorem (Hibbeler 2001):

$$\begin{aligned} \Delta u_1 &= \frac{\partial U}{\partial m_4}, \Delta u_2 = \frac{\partial U}{\partial m_5}, \Delta u_3 = \frac{\partial U}{\partial m_6}, \\ \Delta u_4 &= \frac{\partial U}{\partial f_1}, \Delta u_5 = \frac{\partial U}{\partial f_2}, \Delta u_6 = \frac{\partial U}{\partial f_3} \end{aligned} \tag{22}$$

Afterward, the relationship that links the displacements with the applied wrenches can be determined as

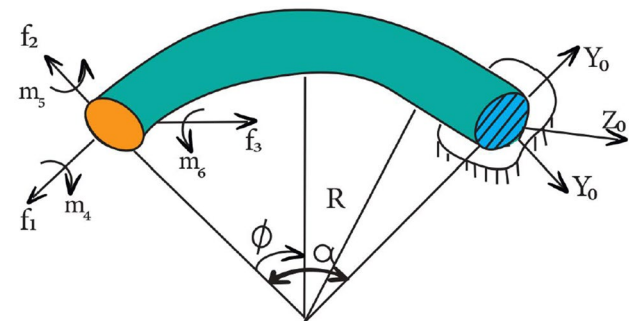


Fig. 4 A curved beam element acted upon by external wrenches

$$\begin{bmatrix} \Delta u_1 \\ \Delta u_2 \\ \Delta u_3 \\ \Delta u_4 \\ \Delta u_5 \\ \Delta u_6 \end{bmatrix} = \begin{bmatrix} C_{11} & C_{12} & 0 & 0 & 0 & C_{16} \\ C_{12} & C_{22} & 0 & 0 & 0 & C_{26} \\ 0 & 0 & C_{33} & C_{34} & C_{35} & 0 \\ 0 & 0 & C_{34} & C_{44} & C_{45} & 0 \\ 0 & 0 & C_{35} & C_{45} & C_{55} & 0 \\ C_{16} & C_{26} & 0 & 0 & 0 & C_{66} \end{bmatrix} \begin{bmatrix} m_4 \\ m_5 \\ m_6 \\ f_1 \\ f_2 \\ f_3 \end{bmatrix} \tag{23}$$

The elements of matrix K_{L-1}^θ are

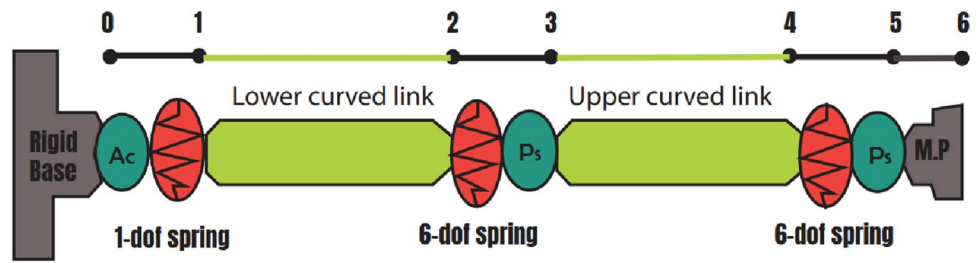
$$\begin{aligned} C_{11} &= \frac{R}{2} \left(\frac{s_1}{GI_x} + \frac{s_2}{EI_y} \right), C_{22} = \frac{R}{2} \left(\frac{s_2}{GI_x} + \frac{s_1}{EI_y} \right); \\ C_{12} &= \frac{s_8 R}{2} \left(\frac{1}{GI_x} - \frac{1}{EI_y} \right), c_{16} = \frac{R^2}{2} \left(\frac{s_2}{EI_y} - \frac{s_7}{EI_x} \right); \\ c_{26} &= \frac{R^2}{2} \left(\frac{s_4}{GI_y} - \frac{s_2}{EI_y} \right); c_{33} = \frac{R\alpha_L}{EI_z}; c_{35} = \frac{s_5 R^2}{EI_z} \\ c_{35} &= \frac{s_6 R^2}{EI_z}; c_{44} = \frac{R}{2A} \left(\frac{s_1}{E} + \frac{s_2}{G} \right) + \frac{s_3 R^3}{2EI_z}; \\ c_{45} &= \frac{s_8 R}{2A} \left(\frac{1}{E} - \frac{1}{G} \right) + \frac{s_4 R^3}{2EI_z}, c_{55} = \frac{R}{2A} \left(\frac{s_1}{E} + \frac{s_2}{G} \right) + \frac{s_2 R^3}{2EI_z}; \\ c_{66} &= \frac{R\alpha_L}{GA} + \frac{R^3}{2} \left(\frac{s_3}{GI_x} + \frac{s_2}{EI_y} \right) \\ s_1 &= \alpha_L + \sin \alpha_L \cdot \cos \alpha_L \\ s_2 &= \alpha_L - \sin \alpha_L \cdot \cos \alpha_L \\ s_3 &= 3 \cdot \alpha_L + \sin \alpha_L \cdot \cos \frac{\alpha_L}{2} - 4 \sin \alpha_L \\ s_4 &= 1 - \cos \alpha_L - \sin^2 \frac{\alpha_L}{2} \\ s_5 &= \sin \alpha_L - \alpha_L \\ s_6 &= \sin \alpha_L - \alpha_1 \\ s_7 &= 2 \cdot \sin \alpha_L - \alpha_L - \sin \alpha_L \cdot \cos \alpha_L \\ s_8 &= -\sin^2 \alpha_L \end{aligned}$$

Matrix A denotes the area of the cross section, E the Young’s modulus, $G = \frac{E}{2} \cdot (1 + \nu)$ is the shear modulus with the Poisson ratio, and $I_x, I_y,$ and I_z are moments of inertia.

3.2 Matrix Structural Analysis (MSA)

The MSA technique is also known as the direct stiffness method (DSM) or the displacement method. It mainly consists in deriving complex structures in individual parts, concerning all possible properties, namely the rigid or flexible support of the mechanism, the rigid or flexible connections, and the passive or active joints. For this reason, MSA-based stiffness analysis provides an easy-to-understand method with step-by-step details. Firstly, we decompose the coaxial SPM into four main parts (fixed and mobile platforms, robot links, type of robot joints, and active or passive joints) as shown in Fig. 5. One of the many advantages that mechanism’s can offer is

Fig. 5 Connections between the manipulator links and base



their symmetry, so we simply derive the MSA technique on a single leg of the kinematic manipulator.

3.3 Modeling of Flexible Links

According to Fig. 5, the links 1–2 and 3–4 are presented as flexible links, and the links under the loading forces are described by

$$\begin{bmatrix} 0_{5 \times 6} & 0_{5 \times 6} & \lambda_{1,2}^r & -\lambda_{1,2}^r \\ I_{6 \times 6} & 0_{6 \times 6} & 0_{6 \times 6} & 0_{5 \times 6} \\ \lambda_{1,2}^e & 0_{5 \times 6} & K_{act} \lambda_{1,2}^e & -K_{act} \lambda_{1,2}^e \end{bmatrix} \begin{bmatrix} W_1 \\ W_2 \\ \Delta t_1 \\ \Delta t_2 \end{bmatrix} = \begin{bmatrix} 0 \\ 0 \\ 0 \\ 0 \end{bmatrix} \quad (24)$$

where K_{11} , K_{12} , K_{21} , and K_{22} stand for (6×6) stiffness matrices, w_i and w_j are the applied wrenches, and Δ_i and Δ_j are the link deflections. In our case study, Eq. (24) can be given as

$$\begin{bmatrix} -I_{6 \times 6} & 0_{6 \times 6} & 0_{6 \times 6} & 0_{6 \times 6} & K_{2,3}^{11} & K_{2,3}^{12} & 0_{6 \times 6} & 0_{6 \times 6} \\ 0_{6 \times 6} & -I_{6 \times 6} & 0_{6 \times 6} & 0_{6 \times 6} & K_{2,3}^{12} & K_{2,3}^{22} & 0_{6 \times 6} & 0_{6 \times 6} \\ 0_{6 \times 6} & 0_{6 \times 6} & -I_{6 \times 6} & 0_{6 \times 6} & 0_{6 \times 6} & 0_{6 \times 6} & K_{4,5}^{11} & K_{4,5}^{12} \\ 0_{6 \times 6} & 0_{6 \times 6} & 0_{6 \times 6} & -I_{6 \times 6} & 0_{6 \times 6} & 0_{6 \times 6} & K_{4,5}^{12} & K_{4,5}^{22} \end{bmatrix} \begin{bmatrix} W_2 \\ W_3 \\ W_4 \\ W_5 \\ \Delta t_2 \\ \Delta t_3 \\ \Delta t_4 \\ \Delta t_5 \end{bmatrix} = \begin{bmatrix} 0 \\ 0 \\ 0 \\ 0 \end{bmatrix} \quad (25)$$

3.4 Modeling of Rigid Links

When the flexibility is negligible, rigidity constraints are replaced, and the rigid body presented as link 5–6 can be written in the form

$$[D^{(ij)} \quad -I_{6 \times 6}] \begin{bmatrix} \Delta t_i \\ \Delta t_j \end{bmatrix} = 0_{6 \times 1} \quad (26)$$

where $D^{(ij)}$ denotes the (3×3) skew-symmetric matrix expressed as

$$D^{(ij)} = \begin{bmatrix} I_{3 \times 3} & [d^{(ij)} \times]^T \\ 0_{3 \times 3} & I_{3 \times 3} \end{bmatrix}_{6 \times 6} \quad (27)$$

In a more explicit form, we can describe link 5–6 by

$$\begin{bmatrix} 0_{6 \times 6} & 0_{6 \times 6} & D_{6 \times e} & -I_{6 \times 6} \\ I_{6 \times 6} & D_{6,e}^T & 0_{6 \times 6} & 0_{6 \times 6} \end{bmatrix} \begin{bmatrix} W_5 \\ W_6 \\ \Delta t_5 \\ \Delta t_6 \end{bmatrix} = \begin{bmatrix} 0 \\ 0 \end{bmatrix} \quad (28)$$

3.5 Modeling of Elastic Joints

Joint 0–1 is given as an active and flexible joint; this returns to the position of the actuators (motors), and it is described by

$$\begin{bmatrix} W_i \\ W_j \end{bmatrix} = \begin{bmatrix} K_{11}^{(ij)} & K_{12}^{(ij)} \\ K_{21}^{(ij)} & K_{22}^{(ij)} \end{bmatrix}_{12 \times 12} \begin{bmatrix} \Delta t_i \\ \Delta t_j \end{bmatrix} \quad (29)$$

According to the proposed coaxial SPM labeled in Fig. 2, we can write the following equation system:

$$\begin{bmatrix} 0_{5 \times 6} & 0_{5 \times 6} & \lambda_{1,2}^r & -\lambda_{1,2}^r \\ I_{5 \times 6} & I_{5 \times 6} & 0_{5 \times 6} & 0_{6 \times 6} \\ \lambda_{1,2}^e & 0_{5 \times 6} & K_{act} \lambda_{1,2}^e & K_{act} \lambda_{1,2}^e \end{bmatrix} \begin{bmatrix} W_1 \\ W_2 \\ \Delta t_1 \\ \Delta t_2 \end{bmatrix} = \begin{bmatrix} 0 \\ 0 \\ 0 \\ 0 \end{bmatrix} \quad (30)$$

with

$$\lambda^r = \begin{bmatrix} 1 & 0 & 0 & 0 & 0 & 0 \\ 0 & 1 & 0 & 0 & 0 & 0 \\ 0 & 0 & 1 & 0 & 0 & 0 \\ 0 & 0 & 0 & R_{11} & R_{12} & R_{13} \\ 0 & 0 & 0 & R_{21} & R_{22} & R_{23} \end{bmatrix} \quad (31)$$

$$\lambda^e = [0 \ 0 \ 0 \ R_{31} \ R_{32} \ R_{33}] \quad (32)$$

where $R_{i,j}$ are the elements of the predefined rotation matrix in Eq. (1), and K_{act} is the actuator’s stiffness matrix.

3.6 Modeling of Passive Joints

Links 2–3 and 4–5 are connected by passive joints. This allows us to present the following form:

$$B = \begin{bmatrix} 0_{30 \times 6} \\ -I_{6 \times 6} \\ 0_{42 \times 6} \end{bmatrix} \tag{40}$$

$$C = [0_{6 \times 36} \quad I_{6 \times 6} \quad 0_{6 \times 36}] \tag{41}$$

$$D = 0_{1 \times 6} \tag{42}$$

As reported earlier, the global study is described according to a single leg of the coaxial SPM. Thus, the aggregate stiffness matrix can be defined as

$$K_C = \sum_{i=1}^3 K_{Ci} \tag{43}$$

5 Force–Displacement Relationship

To demonstrate the utility of applying kinematic redundancy, which is defined by adding extra links or joints to the kinematic manipulator, the coaxial SPM has been varied in terms of its number of legs. The obtained results should pave the way to reliable structure performance. In addition, a force–displacement relationship is derived with respect to the predefined kinematic constraints. Establishing the translational and rotational deflection part of the joints aims at avoiding undesired situations (damage to the mechanism during its function, kineto-static singularities, etc.) and offers an efficient solution (optimal CAD design, choice of materials, etc.). The physical parameters of aluminum are taken into consideration with a Young’s modulus of $2.2 \cdot 10^9$ (Pa), a Poisson ratio of $\eta = 0.37$, link thickness (L_{thk}) of 10^{-2} , cross-sectional area of the link $A = L_{thk}^2$ (m^2), and actuator stiffness K_{act} of 10^6 ($\frac{N}{rad}$). The moment of inertia at the origin for both links is defined with the following expressions: $I_{xx1} = I_{xx2} = 4607.684$ ($g.mm^2$), $I_{yy1} = I_{yy2} = 2.829 \times 10^4$ ($g.mm^2$) and, $I_{zz1} = I_{zz2} = 2.772 \times 10^4$ ($g.mm^2$). The applied wrenches

Table 1 Relationship between deflection components (translation and rotation) and kinematic redundancy

Max and Min deflection in x, y, and z axes	For $i = 3$	For $i = 4$	For $i = 5$
max Δp_x	0.1900	0.1233	0.1212
Max Δp_y	0.1563	0.098	0.1007
Max Δp_z	0.0583	0.0454	0.0358
Max $\Delta \varphi_x$	0.003	0.0015	0.0014
Max $\Delta \varphi_y$	0.0233	0.0121	0.0144
Max $\Delta \varphi_z$	0.0222	0.0072	0.0170
Min Δp_x	0.0498	0.0443	0.0327
Min Δp_y	0.0388	0.0380	0.0280
Min Δp_z	0.0384	0.0310	0.0217
Min $\Delta \varphi_x$	0.0153	0.0082	0.008
Min $\Delta \varphi_y$	0.0113	0.0075	0.0089
Min $\Delta \varphi_z$	0.0032	0.0024	0.0110

take the vector values $W_{ect} = [30N, 30N, 30N, 0N.m, 0N.m, 0N.m]$. Figures 6, 8, and 10 show the obtained translation joint deflection within x, y, and z components, respectively, while Figs. 7, 9, and 11 represent rotation joint deflection within α_x and α_y .

Case 1: MSA-based stiffness matrices of the three-DOF SPM with parameters as ($i = 3$ where i represents the number of legs, $\beta_1 = 0^\circ$, $\beta_2 = 90^\circ$, $\alpha_1 = 90^\circ$, and $\alpha_2 = 90^\circ$)

$$K_{global} = 10^2 \times \begin{bmatrix} 4.3 \cdot 10^3 & -5.62 \cdot 10^2 & 13.56 & 1.79 \cdot 10^2 & 2.22 \cdot 10^2 & -9.5 \\ -5.62 \cdot 10^2 & 5.07 \cdot 10^3 & 2.8 \cdot 10^2 & 1.31 \cdot 10^2 & 2.1 \cdot 10^2 & 0.153 \\ 13.56 & 2.8 \cdot 10^2 & 6.13 \cdot 10^3 & -8.5 & 0.227 & 77.16 \\ 1.79 \cdot 10^2 & 1.31 \cdot 10^2 & -8.5 & 9.45 \cdot 10^2 & -43.53 & 1.52 \\ 2.22 \cdot 10^2 & 2.09 \cdot 10^2 & 0.227 & -43.53 & 1.96 \cdot 10^2 & -2.13 \\ -9.46 & 0.153 & 77.16 & 1.52 & 2.13 & 58.9 \end{bmatrix} \tag{44}$$

Case 2: MSA-based stiffness matrices of the three-DOF SPM with parameters as ($i = 4$ where i represents the number of legs, $\beta_1 = 0^\circ$, $\beta_2 = 90^\circ$, $\alpha_1 = 90^\circ$, and $\alpha_2 = 90^\circ$)

$$K_{global} = 10^2 \times \begin{bmatrix} 4.67 \cdot 10^3 & -1.31 \cdot 10^3 & -81.08 & 2.95 \cdot 10^2 & 2.6 \cdot 10^2 & -10.10 \\ -1.31 \cdot 10^3 & 6.59 \cdot 10^3 & 4.71 \cdot 10^2 & -92.17 & 1.17 \cdot 10^2 & 1.47 \\ -81.09 & 4.71 \cdot 10^2 & 7.83 \cdot 10^3 & -4.03 & -15.10 & 77.42 \\ 2.96 \cdot 10^2 & -92.17 & -4.03 & 1.26 \cdot 10^3 & -10.97 & 2.67 \\ 2.6 \cdot 10^2 & 1.16 \cdot 10^2 & -15.10 & -1.09 \cdot 10^2 & 3.58 \cdot 10^2 & -4.96 \\ -10.10 & 1.47 & 77.42 & 2.67 & -4.97 \cdot 10^2 & 58.9 \end{bmatrix} \tag{45}$$

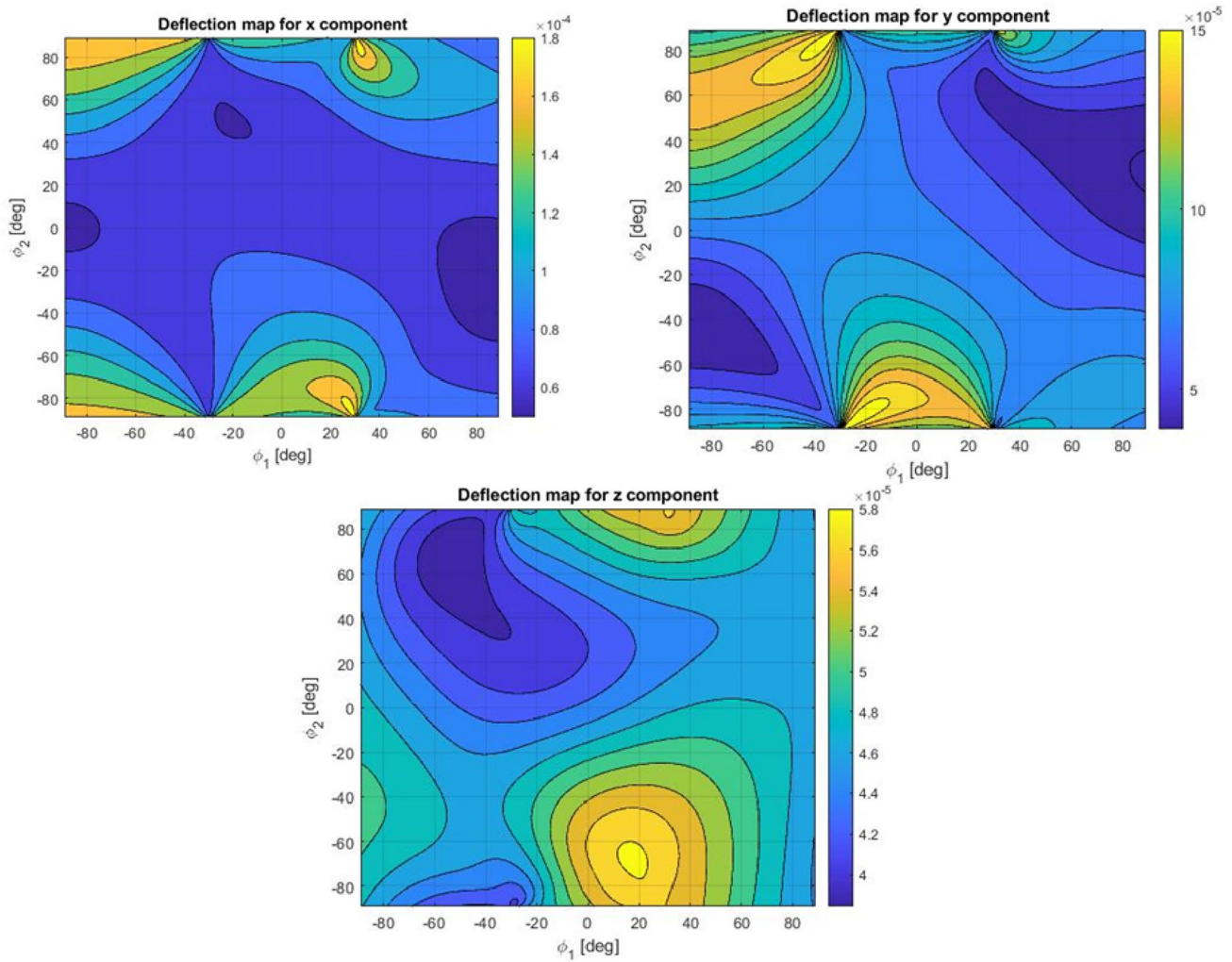


Fig. 6 Joint deflection in x, y, and z axes for the translation part case 1

Case 3: MSA-based stiffness matrices of the three-DOF SPM with parameters as ($i = 5$ where i represents the number of legs, $\beta_1 = 0^\circ$, $\beta_2 = 90^\circ$, $\alpha_1 = 90^\circ$, and $\alpha_2 = 90^\circ$)

From the three cases, it can be noted that the rigidity matrix of the kinematic manipulator gets enlarged whenever the robot gains more links. Furthermore, the robot’s joint deflec-

$$K_{global} = 10^2 \times \begin{bmatrix} 6.02 \cdot 10^3 & -1.71 \cdot 10^3 & -3.46 \cdot 10^2 & 3.73 \cdot 10^2 & 2.82 \cdot 10^2 & 30.90 \\ -1.71 \cdot 10^3 & 7.97 \cdot 10^3 & 8.71 \cdot 10^2 & 1.26 \cdot 10^2 & 2.18 \cdot 10^2 & 1.75 \cdot 10^2 \\ -3.46 \cdot 10^2 & 8.71 \cdot 10^2 & 10^3 & 2.62 \cdot 10^2 & 3.92 & 1.16 \cdot 10^2 \\ 3.73 \cdot 10^2 & 1.25 \cdot 10^2 & 2.61 \cdot 10^2 & 1.57 \cdot 10^3 & -92.10 & 41.07 \\ 2.82 \cdot 10^2 & 2.18 \cdot 10^2 & 3.92 & -92.1 & -3.68 \cdot 10^2 & 11.85 \\ 30.90 & 1.76 \cdot 10^2 & 1.17 \cdot 10^2 & 41.07 & 11.85 & 88.10 \end{bmatrix} \quad (46)$$

MSA technique has been applied to study the robot’s stiffness behavior. Additionally, kinematic redundancy was investigated by adding rigid links (legs) to the regular SPM form, as presented in case 1, case 2, and case 3 with varying numbers of three legs, four legs, and five legs, respectively.

tion is given with regard to the applied force, and as a result, Figs. 6–11 stand for joint deflection of both parts, translation, and rotation deflection of the different cases of study. It is noteworthy to point out that as long as the kinematic manipulator gains links, the deflection gets reduced. From the graphical representation, the blue areas stand for the

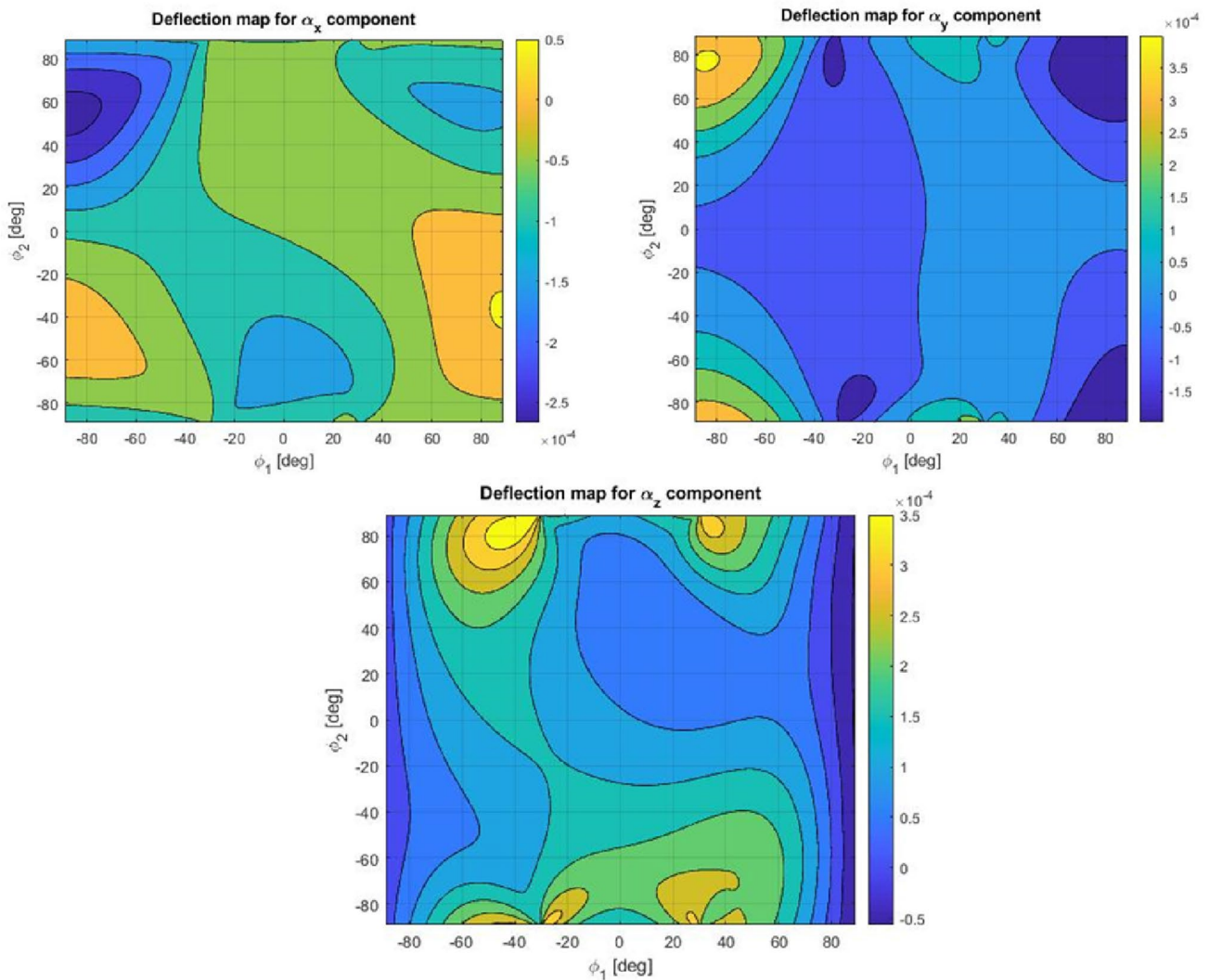


Fig. 7 Joint deflection in x, y, and z axes for the rotation part case 1

lowest parts of joint deflection, while the yellow areas represent the critical ones that must be avoided in accordance with the robot’s orientation (ϕ_1, ϕ_2) . Based on the numerical calculation, Table 1 presents the maximum and minimum deflection values on both parts, the translation part along the $x, y,$ and z axes, and the rotation part along $\alpha_x, \alpha_y,$ and α_z . The derived results demonstrate the advantages of using the kinematic redundancy, of which the deflection has been decreased.

6 Comparative Study of MSA with VJM in Modeling SPM Stiffness

In this section, a comparison study is conducted to validate the proposed method in this paper with VJM. The robot’s physical and mechanical parameters were previously defined in Sect. 5.

Axiomatically, the deformation has an impact on any mechanical structure; it does not exclusively affect its body, but also its links and joints. Accordingly, the virtual joint method (VJM) concerns the study of the deformations of the mechanical structure by considering virtual spring joints.

In the following section, the mathematical model using VJM is presented through the kineto-static of the i th leg and which can be given as follows:

$$\begin{bmatrix} S_{\theta}^i & J_q^i \\ J_q^{iT} & 0_{2 \times 2} \end{bmatrix} \cdot \begin{bmatrix} f_i \\ \Delta q_i \end{bmatrix} = \begin{bmatrix} S_0^i \\ 0_{2 \times 1} \end{bmatrix} \tag{47}$$

where $S_{\theta}^i = J_{\theta}^i \cdot (k_{\theta}^i)^{-1} \cdot J_{\theta}^{iT}$ stands for the compliance of the spring with the frame reference R_0 on the mobile platform, where J_q^{iT} is the Jacobian matrix. Furthermore, $(k_{\theta}^i)^{-1}$ describes the stiffness matrix of both the actuators and the virtual springs, which takes the following equation:

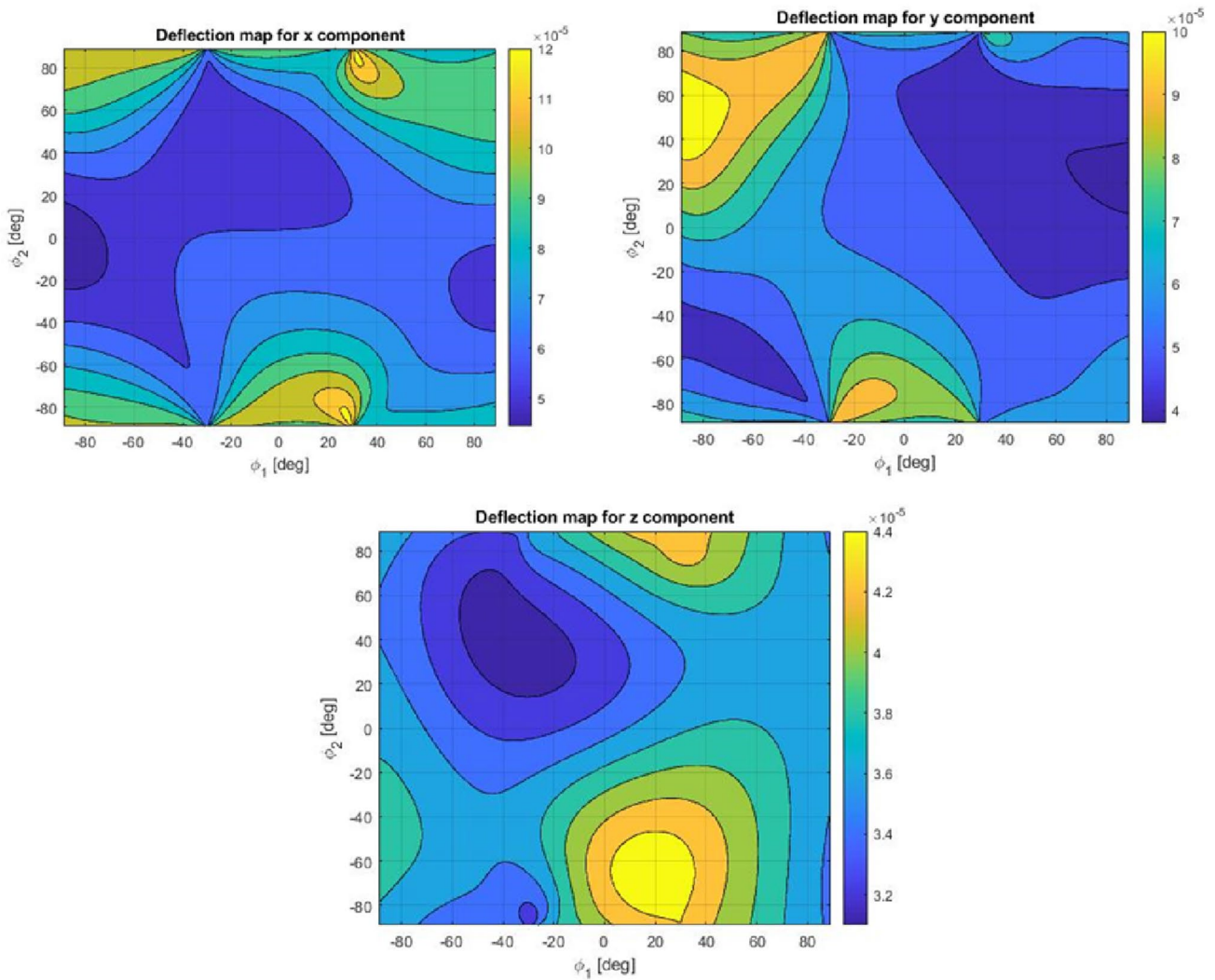


Fig. 8 Joint deflection in x, y, and z axes for the translation part case 2

$$k_{\theta}^i = \begin{bmatrix} k_{act}^i & 0_{1 \times 6} & 0_{1 \times 6} \\ 0_{6 \times 1} & k_{L1}^i & 0_{2 \times 2} \\ 0_{6 \times 1} & 0_{6 \times 6} & k_{L2}^i \end{bmatrix} \quad (48)$$

where k_{act}^i denotes the i th actuator stiffness, while k_{L1}^i and k_{L2}^i are the stiffness matrices of the proximal and distal link

of the i th leg. The Cartesian matrix of the i th leg takes the following equation:

$$k_{Li}^i = \begin{bmatrix} S_{\theta}^i & J_q^i \\ J_{\theta}^{iT} & 0_{2 \times 2} \end{bmatrix} \quad (49)$$

and

$$k_{L1}^i = k_{L2}^i = \begin{bmatrix} 4,96.10^5 & -1,47.10^5 & 6,97.10^2 & -1,15.10^3 & -2.10^3 & 2,70.10^4 \\ -1,47.10^5 & 4,9.10^5 & -2,32.10^3 & 3,82.10^3 & 7.10^3 & -8,05.10^3 \\ 6,97.10^2 & -2,32.10^3 & 2,8.10^5 & -6,2.10^3 & -1,37.10^4 & 38,07 \\ -1,15.10^3 & 3,82.10^3 & -6,2.10^3 & 4.10^4 & 2,3.10^4 & -62,76 \\ -2.10^3 & 7.10^3 & -1,37.10^4 & 2,3.10^4 & 4.10^4 & -1,11.10^2 \\ 2,70.10^4 & -8,05.10^3 & 38,07 & -62,76 & -1,11.10^2 & 2,8.10^5 \end{bmatrix} \quad (50)$$

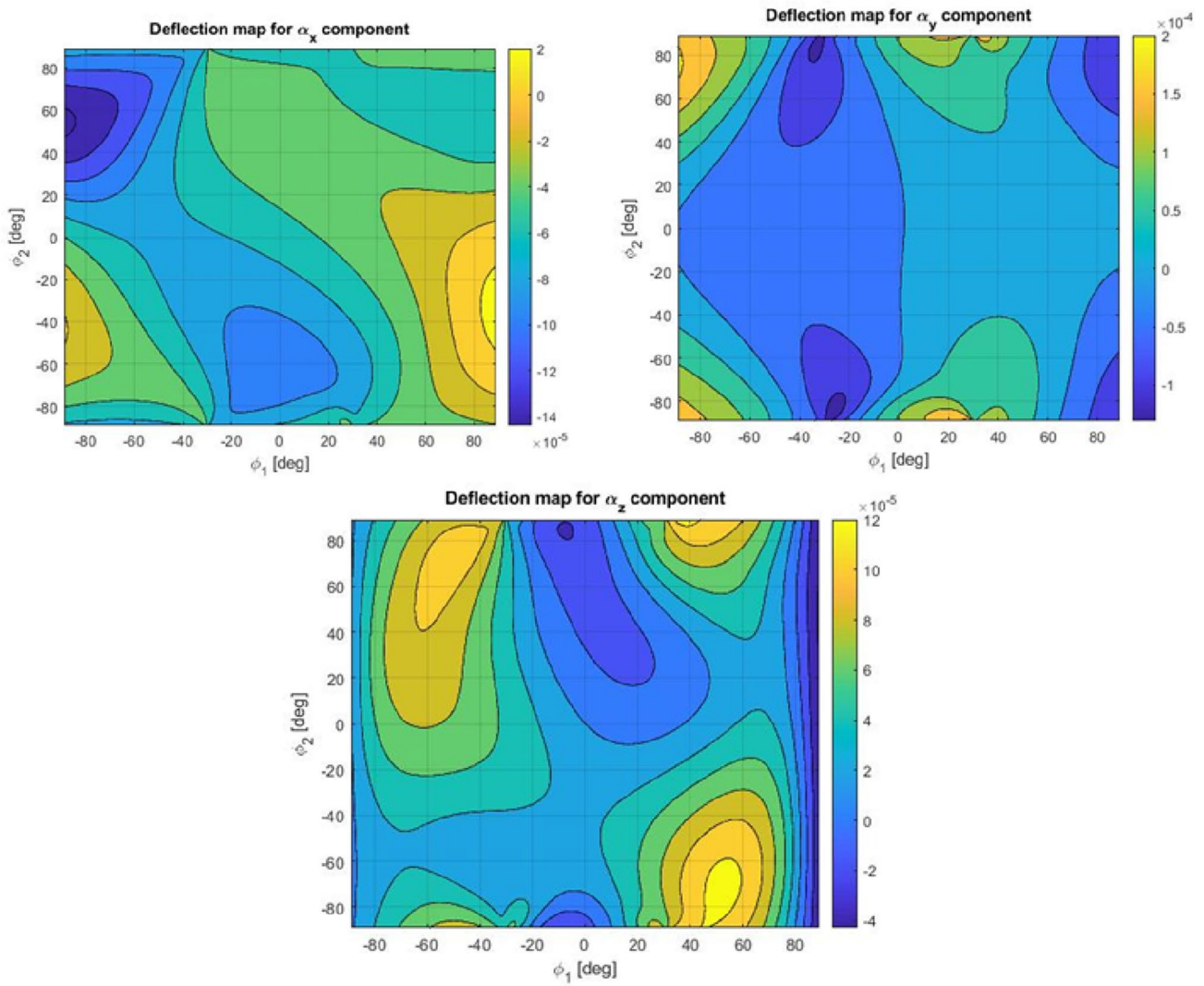


Fig. 9 Joint deflection in x, y, and z axes for the rotation part case 2

As a consequence, the global stiffness matrix of the SPM is defined as

$$k_{Global(VJM)} = \sum_{i=1}^n k_i \tag{51}$$

And the SPM deformation screw is found as (Wu et al. 2014)

$$S_\theta = [\Delta\varphi^T \ \Delta p^T] = k^{-1} \cdot f \tag{53}$$

$$k_{Global(VJM)} = 10^2 \cdot \begin{bmatrix} 4,1 \cdot 10^3 & -3,96 \cdot 10^2 & -9,11 & 1,38 \cdot 10^2 & 1,84 \cdot 10^2 & -6,54 \\ -3,96 \cdot 10^2 & 4,45 \cdot 10^3 & 1,7 \cdot 10^2 & 1,29 \cdot 10^2 & 2 \cdot 10^2 & 0 \\ -9,11 & 1,7 \cdot 10^2 & 6,11 \cdot 10^3 & -2,3 & 0 & 56,18 \\ 1,38 \cdot 10^2 & 1,29 \cdot 10^2 & -2,3 & 9,44 \cdot 10^2 & -35,49 & 0 \\ 1,84 \cdot 10^2 & 2 \cdot 10^2 & 0 & -35,49 & 1,83 \cdot 10^2 & 0 \\ -6,54 & 0 & 56,18 & 0 & 0 & 56,48 \end{bmatrix} \tag{52}$$

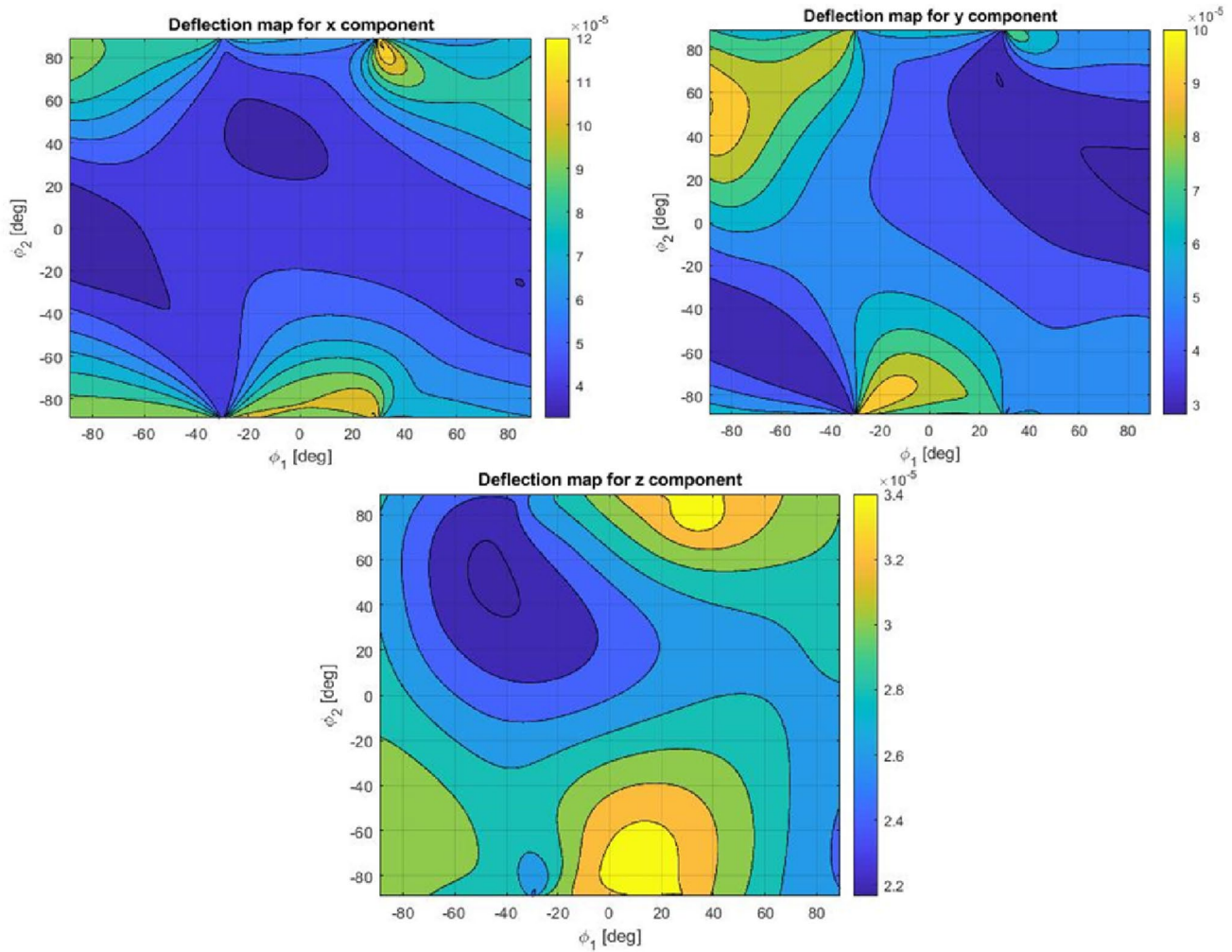


Fig. 10 Joint deflection in x, y, and z axes for the rotation part case 3

where $\Delta\varphi$ and Δp are the orientation and translation displacement, respectively, where f is a (6×1) vector that represents the external wrenches.

Remarkably, from Tables 1, 2, and 3, the obtained values from both methods show that the MSA technique provides quite similar results. Based on the simulated results using MSA, the robot's behavior, namely the joints' deflection, has acceptable values according to the simulation results. In this respect, MSA can be considered as a reliable method to model the complexity of the studied robot. It is noteworthy that the comparative study is mainly based on case 1 for $i = 3$. The relative error (%) between MSA and VJM methods can be mathematically represented as follows:

$$\varepsilon = \left| \frac{\delta_{MSA} - \delta_{VJM}}{\delta_{VJM}} \right| \cdot 100\% \quad (54)$$

noting that δ_p and δ_φ signify the translation and orientation displacement, respectively. The average relative error for δ_p is around (1.48%), and the average error for δ_φ is approximately (3.75%). As shown in Fig. 12, the obtained results from both VJM and MSA methods are considerably similar, which supports the proposed theory.

7 Conclusions

This paper investigates a coaxial spherical parallel manipulator (SPM) using the matrix structural analysis (MSA) method. The proposed numerical approach is mainly established based

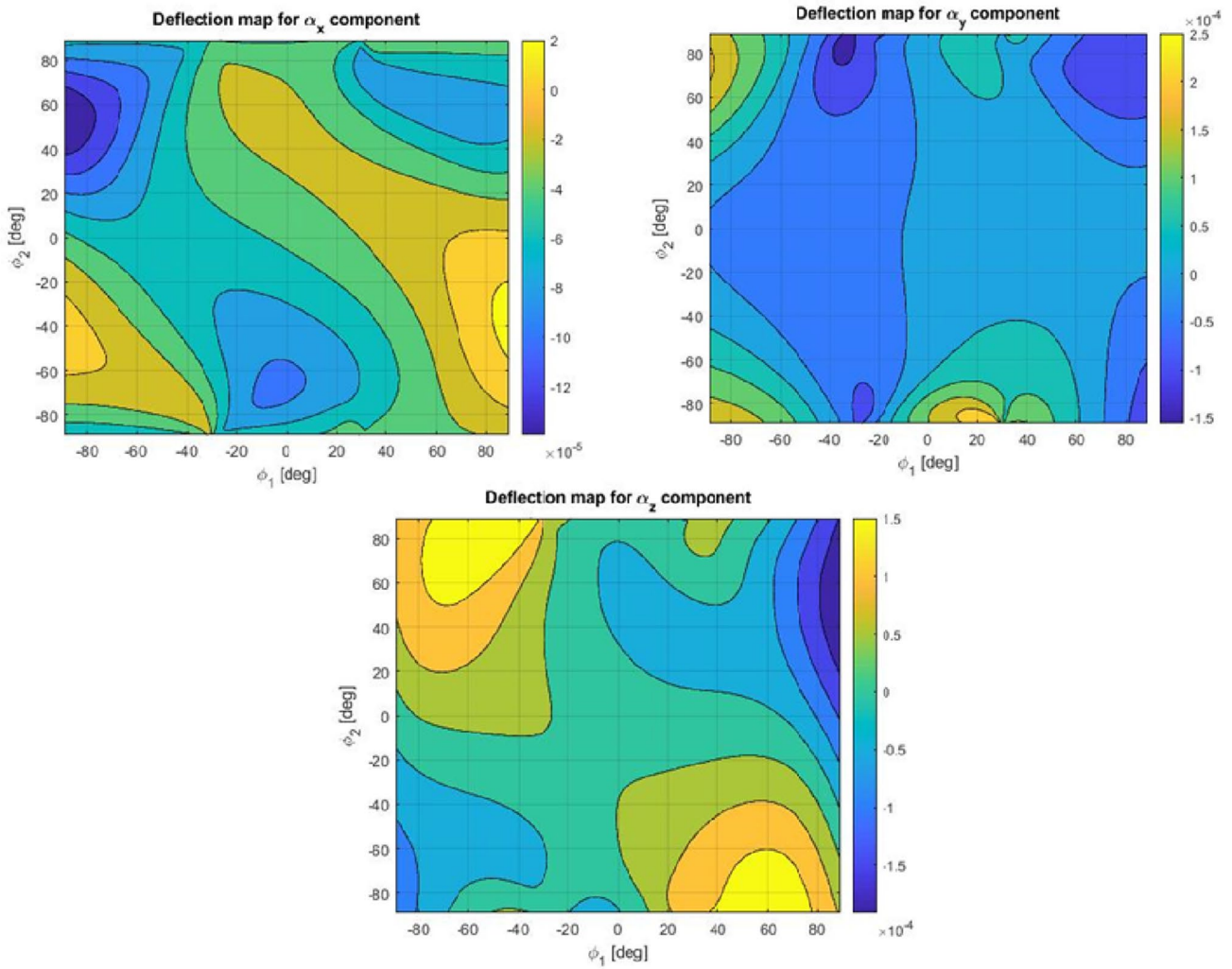


Fig. 11 Joint deflection in x, y, and z axes for the rotation part case 3

Table 2 Max and Min translational deflection

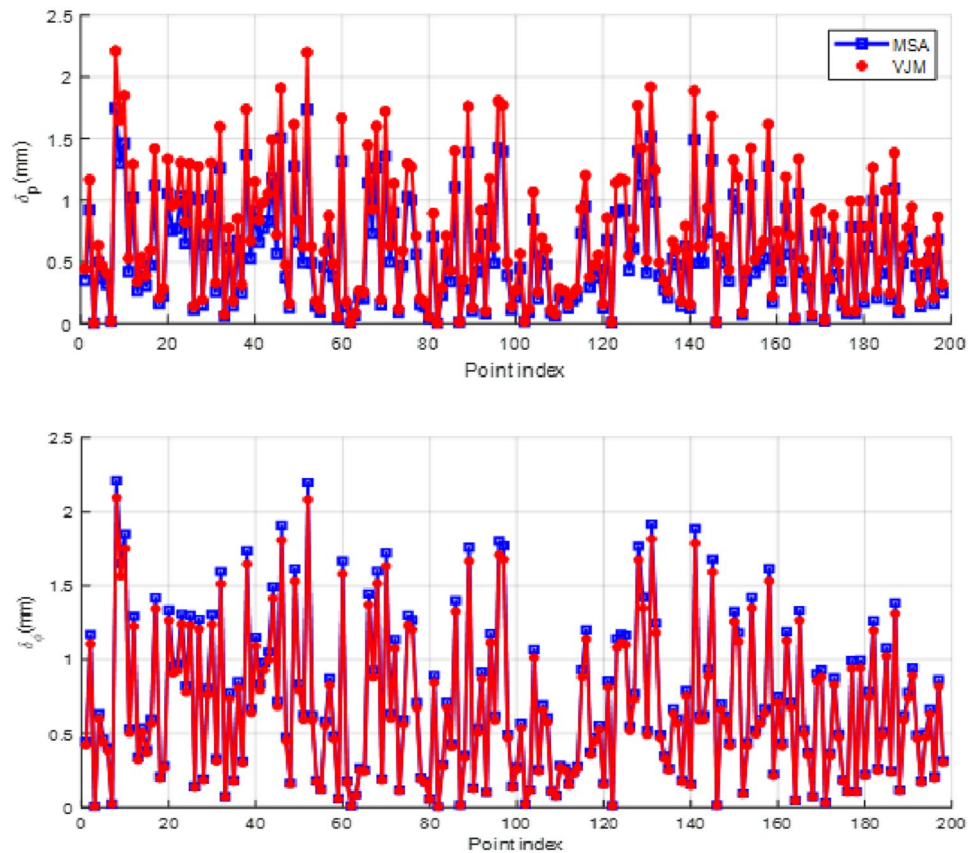
Max	$\Delta p_x(mm)$	$\Delta p_y(mm)$	$\Delta p_z(mm)$	Min	$\Delta p_x(mm)$	$\Delta p_y(mm)$	$\Delta p_z(mm)$
0.1685	0.1042	0.4096	0.029	0.0124	0.0022		

Table 3 Max and Min rotational deflection

Max	$\Delta p_x(rad)$	$\Delta p_y(rad)$	$\Delta p_z(rad)$	Min	$\Delta p_x(rad)$	$\Delta p_y(rad)$	$\Delta p_z(rad)$
0.00106	0.006	0.0013	0.0047	0.0017	0.0136		

on Castigliano’s theorem. This theorem is adopted to derive the robot’s curved beams included in the stiffness matrix. The MSA technique offers a simple and real time-based method that can deal with multiple cases involving rigid and flexible body structures, passive and active joints, and rigid and elastic joints, as well as a variety of the robot’s kinematic chains, namely serial, parallel, and hybrid kinematic architectures. This paper provides an elaborate step-by-step mathematical calculation starting with the robot’s kinematics modeling and ending with the stiffness modeling, which paves the way to a thorough understanding of the studied robot. Additionally, kinematic redundancy is represented based on adding extra links to the

Fig. 12 Comparison of the translation and rotation deflections



uniform 3-RRR coaxial SPM. Interestingly, the obtained results show a higher stiffness matrix by increasing the robot's redundant links. Moreover, joint deflection is represented according to an applied external loading (forces). It is remarkable that joint deflection in both components, translational and rotational parts, decreases when adding extra links, which proves the theory developed in this work. To validate the efficiency of the proposed method, MSA is purposefully compared with VJM.

Acknowledgements A warm thanks to my co-authors for the considerable help regarding the paper's content in substance and in form, in particular that it was written using LaTeX software. I also appreciate my co-authors' help in revising such lengthy mathematical equations.

Author Contributions The authors contributed equally.

Funding No funding sources.

Data Availability Statement Data are available upon request.

Declarations

Conflicts of interest No conflict of interest.

References

- Azulay H, Mahmoodi M, Zhao R, Mills JK, Benhabib B (2014) Robotics and computer-integrated manufacturing comparative analysis of a new 3 Å PPRS parallel kinematic mechanism. *Robot Comput Integ Manuf* 30(4):369–378. <https://doi.org/10.1016/j.rcim.2013.12.003>
- Bonev IA, Ryu J (2001) New approach to orientation workspace analysis of 6-DOF parallel manipulators. *Mech Mach Theory* 36(1):15–28. [https://doi.org/10.1016/S0094-114X\(00\)00032-X](https://doi.org/10.1016/S0094-114X(00)00032-X)
- Bonev IA, Zlatanov D, Gosselin CM (2002) Advantages of the modified Euler angles in the design and control of PKMs. In: *proceeding of parallel kinematic machines international conference*, pp 171–188
- Cammarata A (2016) Unified formulation for the stiffness analysis of spatial mechanisms. *MAMT* 105:272–284. <https://doi.org/10.1016/j.mechmachtheory.2016.07.011>
- Christensen S, Bai S (2018) Kinematic analysis and design of a novel shoulder exoskeleton using a double parallelogram linkage. *J Mech Robot* 10(4):1–10. <https://doi.org/10.1115/1.4040132>
- Deblaise D, Hernot X, Maurine PA (2006) Systematic analytical method for PKM stiffness matrix calculation. *Delta* (May), pp 4213–4219
- Gosselin CM, Lavoie E (1993) On the kinematic design of spherical three-degree-of-freedom parallel manipulators. *Int J Robot Res* 12(4):394–402. <https://doi.org/10.1177/027836499301200406>
- Gosselin CM, Sefrioui J, Richard MJ (1994) On the direct kinematics of spherical three-degree-of-freedom parallel manipulators of general architecture. *J Mech Des Trans ASME* 116(2):594–598. <https://doi.org/10.1115/1.2919419>
- Hibbeler RC (2001) *Mechanics of Materials* Eighth Edition,

- Klimchik A (2018) ScienceDirect MSA-technique MSA-technique for for stiffness stiffness modeling modeling of of manipulators manipulators MSA-technique for stiffness of structures MSA-technique for stiffness of structures MSA-technique for stiffness of. IFAC Papers Online 51(22):37–43. <https://doi.org/10.1016/j.ifacol.2018.11.515>
- Klimchik A, Ambiehl A, Garnier S, Furet B, Pashkevich A (2017) Efficiency evaluation of robots in machining applications using industrial performance measure. Robot Comput Integrat Manufact 48:12–29. <https://doi.org/10.1016/j.rcim.2016.12.005>
- Klimchik A, Pashkevich A, Chablat D (2012) Short papers computational aspects. IEEE Int Conf Adv Intell Mechatron 28(4):955–958
- Klimchik A, Chablat D, Pashkevich A (2019) Advancement of MSA-technique for stiffness modeling of serial and parallel robotic manipulators. In: CISM international centre for mechanical sciences, courses and lectures. https://doi.org/10.1007/978-3-319-78963-7_45
- Li T, Jiang J, Deng H (2017) Analysis of structural characteristics and mobility of planar generalized mechanisms. Iran J Sci Technol Trans Mech Eng 41(1):25–34
- Martinez JA, Ng P, Lu S, Campagna MS, Celik O (2013) Design of Wrist Gimbal : a forearm and wrist exoskeleton for stroke rehabilitation
- Nagai K, Liu ZA (2008) Systematic approach to stiffness analysis of parallel mechanisms, pp 1543–1548
- Niyetkaliyev A, Shintemirov A (2014) An approach for obtaining unique kinematic solutions of a spherical parallel manipulator. In: 2014 IEEE/ASME international conference on advanced intelligent mechatronics, pp. 1355–1360 . IEEE
- Pashkevich A, Chablat D, Wenger P (2009) Stiffness analysis of overconstrained parallel manipulators. Mech Mach Theory 44(5):966–982
- Pashkevich A, Klimchik A, Chablat D (2011) Enhanced stiffness modeling of manipulators with passive joints. Mech Mach Theory 46(5):662–679. <https://doi.org/10.1016/j.mechmachtheory.2010.12.008>
- Pehlivan AU, Lee S, O'Malley MK Mechanical design of RiceWrist-S: A forearm-wrist exoskeleton for stroke and spinal cord injury rehabilitation. In: proceedings of the IEEE RAS and EMBS international conference on biomedical robotics and biomechatronics, pp. 1573–1578 (2012). <https://doi.org/10.1109/BioRob.2012.6290912>
- Piras G, Cleghorn WL, Mills JK (2005) Mechanism and machine theory dynamic finite-element analysis of a planar high-speed. High Precis Parall Manipulat Flexible Links 40:849–862. <https://doi.org/10.1016/j.mechmachtheory.2004.12.007>
- Popov D, Skvortsova V, Klimchik A (2019) Stiffness modeling of 3RRR parallel spherical manipulator. In: CEUR workshop proceedings. vol. 2525
- Saafi H, Laribi MA, Zeghloul S, Ibrahim MY (2013) Development of a spherical parallel manipulator as a haptic device for a teleoperation system: Application to robotic surgery. In: IECON proceedings (industrial electronics conference), pp. 4097–4102. <https://doi.org/10.1109/IECON.2013.6699792>
- Taghaeipour A, Angeles J, Lessard L, Taghvaeipour A (2010) Online computation of the stiffness matrix in robotic structures using finite element analysis. McGill University, Montreal
- Taghvaeipour A, Angeles J, Lessard L (2012) On the elastostatic analysis of mechanical systems. MAMT 58:202–216. <https://doi.org/10.1016/j.mechmachtheory.2012.07.011>
- Tursynbek I, Shintemirov A (2021) Infinite rotational motion generation and analysis of a spherical parallel manipulator with coaxial input axes. Mechatronics. <https://doi.org/10.1016/j.mechatronics.2021.102625>
- Wu G, Bai S, Kepler J (2014) Mobile platform center shift in spherical parallel manipulators with flexible limbs. Mech Mach Theory 75:12–26. <https://doi.org/10.1016/j.mechmachtheory.2014.01.001>
- Wu G, Bai S, Kepler J (2014) Mobile platform center shift in spherical parallel manipulators with flexible limbs. Mech Mach Theory 75:12–26
- Springer Nature or its licensor (e.g. a society or other partner) holds exclusive rights to this article under a publishing agreement with the author(s) or other rightsholder(s); author self-archiving of the accepted manuscript version of this article is solely governed by the terms of such publishing agreement and applicable law.